ACS APPLIED MATERIALS & INTERFACES

Research Article

www.acsami.org

Facile Synthesis of Urchin-like $NiCo_2O_4$ Hollow Microspheres with Enhanced Electrochemical Properties in Energy and Environmentally Related Applications

Xin-Yao Yu,[†,‡] Xian-Zhi Yao,[†,‡,§] Tao Luo,[†] Yong Jia,[†] Jin-Huai Liu,[†] and Xing-Jiu Huang*[,†,§]

[†]Nanomaterials and Environmental Detection Laboratory, Institute of Intelligent Machines, Chinese Academy of Sciences, Hefei 230031, People's Republic of China

[§]Department of Chemistry, University of Science and Technology of China, Hefei 230026, People's Republic of China.

Supporting Information

ABSTRACT: A facile synthesis of novel urchin-like $NiCo_2O_4$ hierarchical hollow microspheres has been developed based on a template-free solvothermal and subsequent calcination method. The growth process of $NiCo_2O_4$ hollow microsphere precursors has been investigated, and a plausible mechanism was proposed. Because of their unique structure and high specific surface area, these $NiCo_2O_4$ hollow microspheres displayed enhanced electrochemical properties in methanol electrooxidation and determination of heavy-metal ions compared with solid urchin-like $NiCo_2O_4$ microspheres, Co_3O_4, and NiO microspheres. The good electrochemical performances suggested that these unique hierarchical $NiCo_2O_4$ hollow microspheres could be promising materials for energy and environmentally related applications.

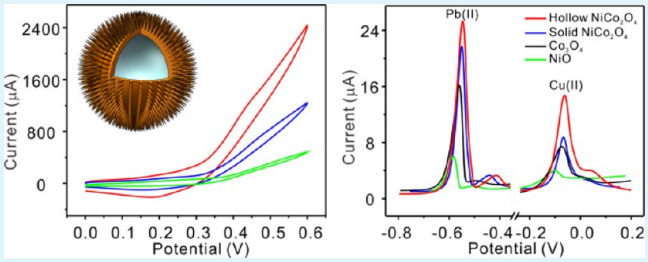

KEYWORDS: *$NiCo_2O_4$, solvothermal, urchin-like, hollow microspheres, methanol electrooxidation, heavy-metal ions*

1. INTRODUCTION

Hollow micro/nanostructured materials with hierarchical structures have attracted much attention in a wide range of potential applications, such as energy storage, catalysis, sensors, drug delivery, and water treatment.[1−8] Over the past decade, numerous hollow micro/nanostructured materials with various morphologies have been synthesized using both template and template-free methods.[1,9] Especially, the template-free method is believed to be more desirable, facile, and scalable than the template method.[10,11] Despite the fact that great effort has been made, it is still a big challenge to produce hierarchical hollow micro/nanostructured mixed-metal oxides with desirable nanoscale building blocks and secondary architectures for energy and environmentally related applications.

$NiCo_2O_4$ as a promising mixed-metal oxide has been widely investigated for potential applications in lithium-ion batteries, supercapacitors, electrocatalysts, and optoelectronic devices.[12−17] In particular, it has been reported that $NiCo_2O_4$ possesses much better electronic conductivity, at least 2 orders of magnitude higher than nickel oxide and cobalt oxide.[18] The high electronic conductivity is beneficial for fast electron transfer in an electrode. Recently, there have been many reports on the synthesis of $NiCo_2O_4$ with various morphologies. Most of these researches focused on the synthesis of $NiCo_2O_4$ nanoarrays on different conductive substrates.[13,14,16,19] In addition, solid urchin-like $NiCo_2O_4$ microspheres with hierarchical structures have also been fabricated.[20,21] Although few reports have used the template method to synthesize hollow nanostructured $NiCo_2O_4$,[14] there are far fewer reports on the fabrication of hollow $NiCo_2O_4$ hierarchical nanostructures using the temple-free method. Hollow $NiCo_2O_4$ nanostructures may greatly improve the performance in electrochemical applications by offering a high specific surface area, short diffusion path for ions or electrons, and efficient channels for mass transport. Therefore, it is highly desirable but challenging to develop a facile, environmentally benign, and template-free method to produce nanostructured $NiCo_2O_4$ with hierarchical hollow structures.

Herein, we report a facile template-free solvothermal method in a mixed solution of isopropyl alcohol (IPA) and water for the construction of hierarchical urchin-like $NiCo_2O_4$ hollow microsphere precursors with nanorods as building blocks. We observed an interesting structural evolution process from solid nanoflake-assembled microspheres to hollow microspheres constructed by nanorods. These $NiCo_2O_4$ hollow microsphere precursors were subsequently converted to $NiCo_2O_4$ hollow spheres with well-preserved structures. Remarkably, the as-synthesized hierarchical urchin-like $NiCo_2O_4$ hollow spheres with a high surface area of 70 m^2 g^{-1} exhibited enhanced electrochemical performances in methanol electrooxidation and determination of heavy-metal ions (HMIs) compared with solid

Received: December 31, 2013
Accepted: February 17, 2014
Published: February 17, 2014

   dx.doi.org/10.1021/am4060707 | ACS Appl. Mater. Interfaces 2014, 6, 3689−3695

urchin-like $NiCo_2O_4$ microspheres, urchin-like Co_3O_4, and urchin-like NiO microspheres.

2. EXPERIMENTAL SECTION

Materials Synthesis. The $NiCo_2O_4$ hollow microsphere precursors were synthesized by a simple solvothermal method. All chemicals were of analytical grade and were used as received without further purification. In a typical synthesis, $Co(NO_3)_2{\cdot}4H_2O$ (0.58 g), $Ni(NO_3)_2{\cdot}6H_2O$ (0.29 g), and urea (3.6 g) were dissolved in a mixture of IPA (15 mL) and water (3 mL). The resulting mixture was stirred for 30 min and then transferred into a 23 mL Teflon-lined stainless-steel autoclave, which was heated at 120 °C for a period of 12 h in an electric oven. The synthesis of the solid $NiCo_2O_4$ microsphere precursors was similar to that of hollow microspheres, except that 0.54 g of urea and 18 mL of water were used. In the synthesis of Co_3O_4 microsphere precursors, $Co(NO_3)_2{\cdot}4H_2O$ (0.58 g) and urea (0.6 g) were dissolved in water (50 mL) and then transferred into a 60 mL Teflon-lined stainless-steel autoclave, which was heated at 100 °C for a period of 12 h. For the synthesis of NiO microsphere precursors, $NiCl_2{\cdot}6H_2O$ (1.296 g) and urea (2.4 g) were dissolved in water (100 mL) and then transferred into a 125 mL Teflon-lined stainless-steel autoclave, which was heated at 100 °C for a period of 12 h. The autoclaves after heating were allowed to cool naturally to room temperature. The precipitates were collected and washed with water and ethanol several times by centrifugation and then dried at 80 °C overnight. All of the as-synthesized intermediate products were calcined at 350 °C in air for 2 h at a ramping rate of 1 °C min^{-1}.

Characterization. X-ray diffraction (XRD) was performed on a D/MaxIIIA X-ray diffractometer, using Cu Kα ($\lambda_{K\alpha_1}$ = 1.5418 Å) as the radiation source. The scanning electron microscopy (SEM) images were taken by a FEI Quanta 200 FEG field-emission scanning electron microscope. Transmission electron microscopy (TEM) image analyses were carried out on a JEM-2010 microscope. The nitrogen adsorption−desorption isotherms at 77 K were measured with a Micromeritics ASAP 2020 M analyzer. The Brunauer−Emmett−Teller (BET) equation was used to obtain the specific surface areas. Electrochemical experiments were recorded using a CHI 660D computer-controlled potentiostat (ChenHua Instruments Co., Shanghai, China). A conventional three-electrode system consisted of a glassy carbon working electrode (GCE; 3 mm diameter), an Ag/AgCl or saturated calomel electrode (SCE) as the reference electrode, and a platinum wire as the counter electrode.

Fabrication of a Modified Electrode. Prior to modification, the bare GCE was sequentially polished with 0.3 and 0.05 μm alumina powder slurries to a mirror shiny surface and then successively sonicated with a 1:1 HNO_3 solution, ethanol, and deionized water for 2 min in order to remove any adsorbed substances on the electrode surface. A total of 10 mg of the as-synthesized materials was dispersed in a mixture of 0.1 mL of Nafion and 0.9 mL of water with ultrasonic agitation to give a homogeneous solution. A total of 10.0 μL (for methanol electrooxidation) or 4.0 μL (for HMI detection) of the homogeneous solution was dripped onto the surface of a freshly polished GCE and then evaporated at room temperature in air.

Electrochemical Measurements. The electrochemical performance of these modified electrodes for methanol oxidation was evaluated using cyclic voltammetry (CV), chronoamperometry, and electrochemical impedance spectroscopy (EIS) measurements with SCE as the reference electrode. The electrolyte for methanol electrooxidation tests was 1 M KOH with 0.5 M methanol. EIS tests were performed at open-circuit potential with an alternating-current amplitude of 10 mV, and the frequency range was from 100 kHz to 10 mHz. The electrochemical detection of HMIs was carried out in square-wave stripping voltammetry (SWASV) mode in 0.1 M NaAc−HAc solution (pH 5.0). A deposition potential of −1.2 V was applied for 120 s to the working electrode under stirring. The SWASV responses were recorded with a step potential of 4 mV, an amplitude of 25 mV, and a frequency of 10 Hz. A desorption potential of 0 V for 120 s was used to remove the residual metals on the surface of the electrodes under stirring conditions.

3. RESULTS AND DISCUSSION

XRD measurement was used to identify the chemical composition and phase of the final products. The obtained diffraction peaks labeled in Figure 1a agreed well with the

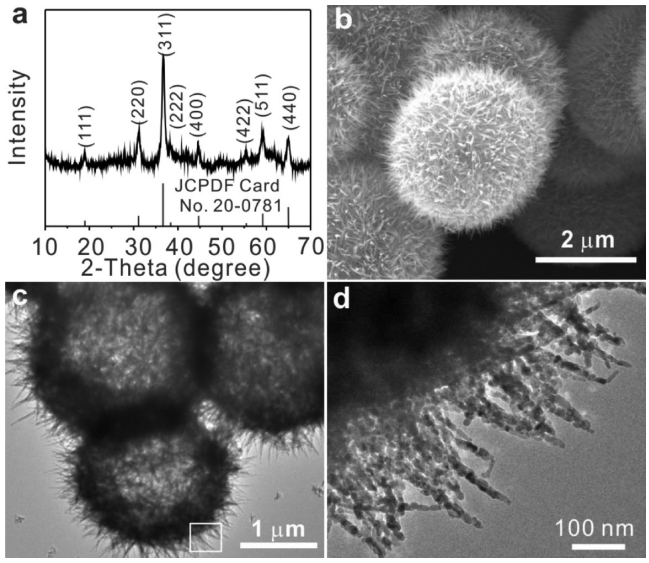

Figure 1. (a) XRD pattern, (b) SEM image, and (c) TEM image of the as-synthesized $NiCo_2O_4$ hollow microspheres. (d) Magnified view of the area marked by a rectangle in panel c.

standard patterns of the spinel $NiCo_2O_4$ phase (JCPDF card no. 20-0781).[16,20] The product was highly pure because no peaks of any impurity phase could be observed from this pattern. The morphology of the as-synthesized $NiCo_2O_4$ microspheres was observed by SEM. As shown in Figure 1b, the obtained microspheres were uniform with a diameter of about 2−3 μm. The urchin-like hierarchical structures with numerous nanorods radially grown on the surface can be clearly seen. As seen from some broken microspheres (Figure S1 in the Supporting Information, SI), it could be observed that the microspheres were hollow. The interior structure of these microspheres was further investigated by TEM (Figure 1c), where a large void space can be clearly seen.

The TEM image (Figure 1d) taken from the marked area of Figure 1c revealed the shell structure of the hollow microspheres. It can be seen that the nanorods with a diameter of about 20 nm and a length of about 300 nm were porous and composed of small nanoparticles. As revealed by the nitrogen adsorption−desorption measurement, the hollow urchin-like microspheres gave rise to a relatively high BET specific surface area of about 70 m^2 g^{-1} with a broad pore-size distribution and a high pore volume of 0.46 cm^3 g^{-1} (Figure 2).

The uncalcined microsphere precursors solvothermally prepared in a mixed solution of IPA (15 mL) and water (3 mL) were characterized by SEM and TEM (Figure 3). It can be observed that there appeared to be no noticeable structural change caused by the calcination process. However, the nanorods on the surface of the microsphere precursors were smooth before calcination (inset in Figure 3). The XRD pattern (Figure S2 in the SI) of the microsphere precursors revealed the diffraction of cobalt−nickel bimetallic carbonate hydroxide.

To investigate the effect of the relative amounts of IPA and water in the mixed solvent, the amount of urea, and the temperature on the product morphology, a series of experi-

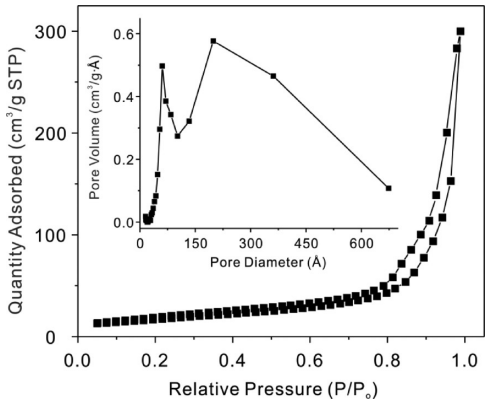

Figure 2. Nitrogen adsorption−desorption isotherm of the $NiCo_2O_4$ hollow microspheres. The inset shows the pore-size distribution from the corresponding adsorption branch.

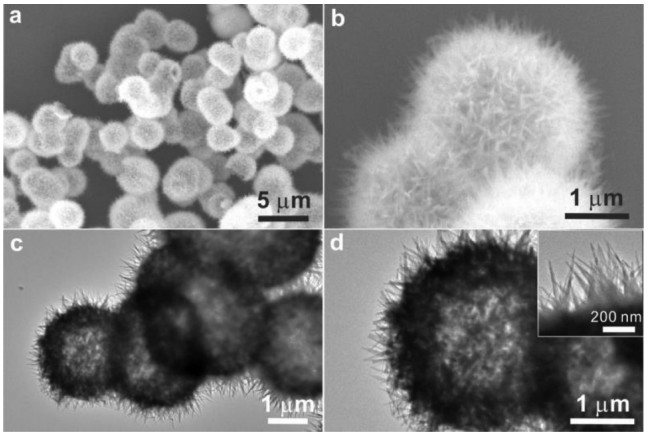

Figure 3. (a and b) SEM and (c and d) TEM images of the hollow $NiCo_2O_4$ precursor. The inset in panel d shows the TEM image of the magnified surface of the microspheres.

ments were carried out by varying the volume ratio of IPA, the amount of urea added, and the solvothermal temperature while keeping other conditions unchanged (Figures S3 and S4 in the SI). In the present solvothermal system, the amount of IPA was found to play an important role in the formation of hollow microsphere precursors. When the amount of IPA was lower than 13 mL or up to 17 mL, no hollow structures were obtained (Figure S3 in the SI). When the urea added was 0.9 or 1.8 g, hollow microsphere precursors were not formed either (Figure S4a,b in the SI). In addition, higher temperature (≥140 °C) led to the collapse of the hollow structures (Figure S4c−e in the SI). These observations suggested that a proper amount of IPA and urea and low solvothermal temperature were essential for the formation of hollow microsphere precursors.

Time-dependent experiments were performed to understand the formation process of such interesting hierarchical urchin-like hollow microsphere precursors. The morphologies of the products after solvothermal treatment for difference time intervals were characterized by SEM. As shown in Figure 4a, solid nanoflake-assembled microspheres were obtained after a reaction duration for 0.5 h. Interestingly, short and not well-developed nanorods were found to assemble onto the surface of the nanoflakes after solvothermal treatment for 3 h (Figure 4b). As shown in Figure 4c, york-shelled microsphere precursors were obtained when the reaction duration was extended to 9 h. After the reaction time was prolonged to 12 h, urchin-like microspheres with completely hollow interior can eventually be obtained (Figure 4d). These results revealed that recrystallization took place at the exterior surface of the microspheres and growth of the nanorod structure on the shell was accompanied by consumption of the interior core. The transformation from solid to hollow particles is usually based on the so-called inside-out Ostwald-ripening process, in which the outer crystalline shells grow on the solid particles accompanied by continuous dissolution and recrystallization of the interior structures.[10,11] The growth of nanorods on the surface of the microspheres and the slight diameter increase of the microspheres with prolonged solvothermal treatment also verified the inside-out Ostwald-ripening process.[11] On the basis of the above experimental observations, a plausible formation mechanism of such hierarchical urchin-like hollow microsphere precursors was proposed (Figure 4e). Cobalt−nickel bimetallic carbonate hydroxide nanoparticles were initially formed by the reaction of metal cations (Co^{2+} and Ni^{2+}) with CO_3^{2-} and OH^- anions slowly released from the hydrolysis of urea in an aqueous solution. Then these nanoparticles self-assembled into solid microspheres composed of flakelike subunits in stage I. After that, the nanoflake-assembled microspheres underwent the first inside-out Ostwald-ripening and recrystallization process, and at the same time, nanorods began to grow on the surface of the nanoflakes (stage II). Upon a further increase in the reaction time, the second inside-out Ostwald-ripening and recrystallization process occurred, which resulted in the formation of a

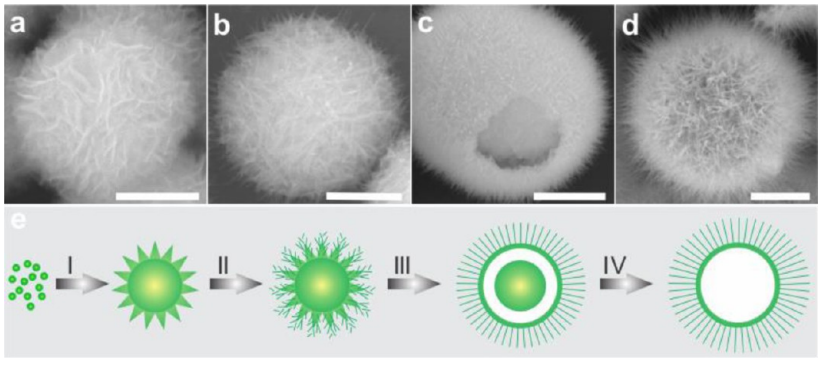

Figure 4. (a−d) SEM images of the products obtained after reaction for (a) 0.5, (b) 3, (c) 9, and (d) 12 h. Scale bar: 1 μm. (e) Schematic illustration of the formation process of the $NiCo_2O_4$ hollow microsphere precursor: (I) self-assembly process; (II) first inside-out Ostwald-ripening and recrystallization process; (III) second inside-out Ostwald-ripening and recrystallization process; (IV) thorough dissolution and recrystallization.

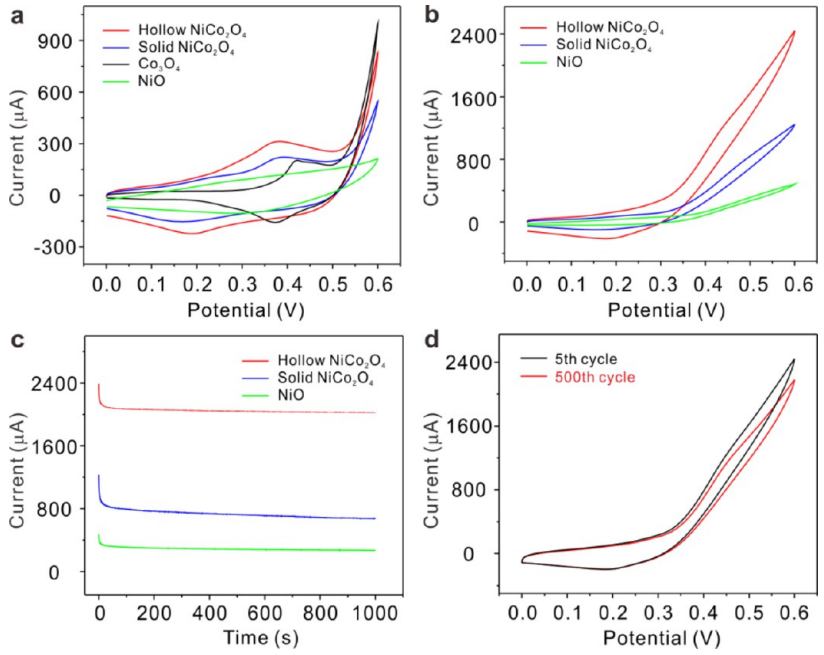

Figure 5. CV curves of $NiCo_2O_4$, Co_3O_4, and NiO modified electrodes in 1 M KOH without (a) and with (b) 0.5 M methanol at a scan rate of 50 mV s^{-1}. (c) Chronoamperometry curves of $NiCo_2O_4$ and NiO modified electrodes in 1 M KOH with 0.5 M methanol at 0.6 V. (d) CV curves of hollow $NiCo_2O_4$ modified electrodes measured at different cycles in 1 M KOH with 0.5 M methanol at a scan rate of 50 mV s^{-1}.

yolk-shelled structure (stage III). The hollowing process continued with longer reaction durations until completely hollow $NiCo_2O_4$ microsphere precursors with well-defined urchin-like structures were obtained (stage IV).

For comparison, solid urchin-like $NiCo_2O_4$ microspheres, urchin-like Co_3O_4, and NiO microspheres were prepared by hydrothermal and subsequent calcination methods. The XRD patterns of solid $NiCo_2O_4$ microsphere precursors, Co_3O_4, and NiO microsphere precursors were similar to that of hollow $NiCo_2O_4$ microsphere precursors with metal carbonate hydroxide phases (Figure S2 in the SI). Their urchin-like morphologies were revealed by SEM images (Figure S5 in the SI). After calcination, all of these microsphere precursors were transformed into metal oxide phases (Figure S6 in the SI) and their morphologies changed little (Figure S7 in the SI). In addition, the specific surface area of the solid $NiCo_2O_4$ microsphere precursors was about 54 m^2 g^{-1} with a narrow size distribution and a pore volume of 0.18 cm^3 g^{-1} (Figure S8 in the SI).

In order to demonstrate the advantages of this unique hollow urchin-like structure, the electrochemical properties of these hollow $NiCo_2O_4$ microspheres were investigated and the performances were compared with solid urchin-like $NiCo_2O_4$ microspheres, urchin-like Co_3O_4, and NiO microspheres. The electrochemical performances of $NiCo_2O_4$, Co_3O_4, and NiO modified electrodes were first investigated using CV in a 1 M KOH solution (Figure 5a). From Figure 5a, we can see that the hollow $NiCo_2O_4$ microsphere modified electrode exhibited the largest enclosed area and the highest redox peak current, indicating its better electrochemical activity than solid urchin-like $NiCo_2O_4$ microspheres, urchin-like Co_3O_4, and NiO microspheres. The charge-transfer processes of solid-state redox couples of Co^{3+}/Co^{2+} (Co_3O_4/CoOOH) and Ni^{3+}/Ni^{2+} (NiO/NiOOH) contributed to these richer redox peaks of spinel $NiCo_2O_4$.[13,22] The charge-transfer resistance of these modified electrodes was also investigated using EIS tests in 1 M KOH. As shown in Figure S9 in the SI, the Nyquist diagram mainly consisted of two parts: a semicircle at high frequency corresponding to the charge-transfer resistance and a trail at low frequency correlated with the redox capacitive behavior of NiO and Co_3O_4.[13] As shown in the inset of Figure S9b in the SI, R_{ct}, C, and R_s in the fitted equivalent circuit corresponded to the charge-transfer resistance in the electrode and at the electrode/electrolyte interface, pseudocapacitance (or redox capacitance), and solution resistance, respectively.[13] The low R_{ct} value corresponding to a small diameter of the semicircle at high frequency implied fast electron or ion transfer.[13] The Nyquist diagram of $NiCo_2O_4$ modified electrodes showed a much smaller semicircle than Co_3O_4 and NiO modified electrodes, suggesting that the charge-transfer rate of $NiCo_2O_4$ was higher than that of Co_3O_4 and NiO (Figure S9 in the SI).

Preliminary investigation of methanol electrooxidation at modified electrodes showed that $NiCo_2O_4$ and NiO modified electrodes exhibited strong oxidation currents in the presence of 0.5 M methanol compared with the CV in the absence of methanol (Figure S10 in the SI). However, the Co_3O_4 modified electrode in the presence of 0.5 M methanol showed little increment in the oxidation current (Figure S10 in the SI), reflecting little electrochemical reactivity for methanol oxidation.[22] Figure 5b showed a comparison of the CV curves obtained at hollow $NiCo_2O_4$, solid $NiCo_2O_4$, and NiO microsphere modified electrodes in the presence of 0.5 M methanol. The methanol oxidation current for the hollow $NiCo_2O_4$ microsphere modified electrode at 0.6 V was about 2 and 5 times that of solid $NiCo_2O_4$ and NiO microsphere modified electrodes, respectively. Furthermore, the hollow $NiCo_2O_4$ microsphere modified electrode exhibited a lower overpotential compared with solid $NiCo_2O_4$ and NiO microsphere modified electrodes. The relatively high oxidation current and low onset potential well evidenced the high electrocatalytic performance of these hollow $NiCo_2O_4$ micro-

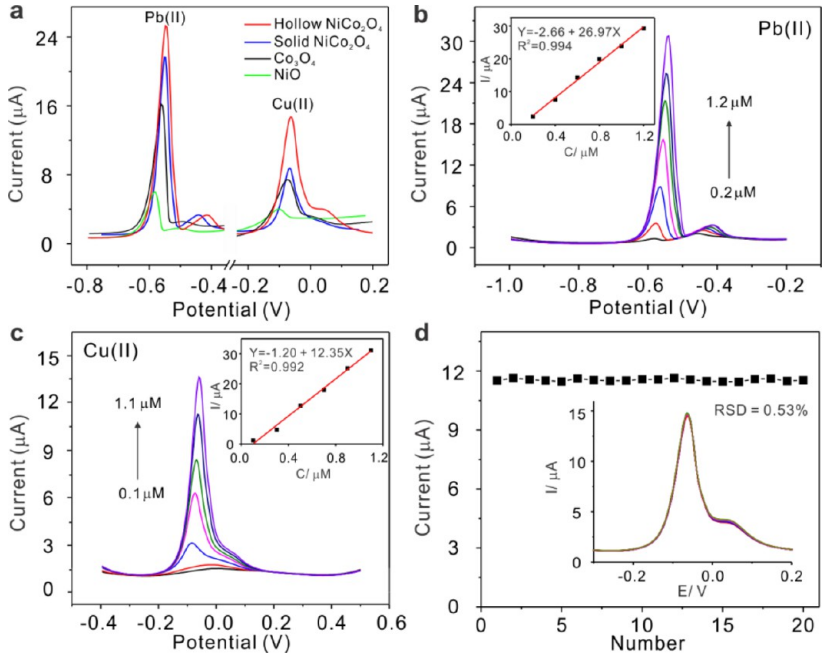

Figure 6. (a) SWASV curves of $NiCo_2O_4$, Co_3O_4, and NiO modified electrodes in response to 1 μM Pb^{II} and 1.1 μM Cu^{II}, respectively. (b and c) SWASV curves and corresponding calibration plots (inset in the panel) of Pb^{II} and Cu^{II} on hollow $NiCo_2O_4$ modified electrodes. (d) Stability study of the hollow $NiCo_2O_4$ modified electrodes toward 1 μM Cu^{II}.

spheres for methanol electrooxidation.[13,22] The methanol electrooxidation stabilities of these metal oxides were measured by chronoamperometry at 0.6 V for consecutive 1000 s (Figure 5c). Although there was a current decay in the first 50 s, the hollow $NiCo_2O_4$ microsphere modified electrodes showed a high stability in the next 950 s. Furthermore, the hollow $NiCo_2O_4$ microsphere modified electrodes exhibited the highest current compared with solid $NiCo_2O_4$ and NiO microsphere modified electrodes. The long-term stability of the hollow $NiCo_2O_4$ microsphere modified electrode was also examined using CV tests. The CV plots were so stable that about 85% of the current density at 0.6 V was retained after 500 cycles (Figure 5d). The above results illustrated that the novel urchin-like $NiCo_2O_4$ hollow structures exhibited high electrochemical reactivity and long-term stability for methanol electrooxidation.

HMIs in water pose a great threat to the health of human beings. The electrochemical method has been regarded as one of the most effective and efficient techniques in the detection of HMIs in water.[23−25] In addition, we have shown that nanoscale metal oxides are excellent modifiers for electrodes for HMI determination considering their higher adsorption capacity for HMIs.[26] To further verify the enhanced electrochemical properties of novel hierarchical $NiCo_2O_4$ hollow microspheres, we then investigated their performance in the electrochemical determination of HMIs. To the best of our knowledge, there are few reports on the utilization of mixed-metal oxides for the electrochemical determination of HMIs. We first examined the SWASV responses of $NiCo_2O_4$, Co_3O_4, and NiO microsphere modified electrodes toward 1 μM Pb^{II} and 1.1 μM Cu^{II} in 0.1 M NaAc-HAc (pH 5.0; Figure 6a). In the detection of Pb^{II}, a strong and well-defined peak at −0.548 V can be clearly seen for hollow $NiCo_2O_4$ microsphere modified electrodes.[26] The peak current obtained from hollow $NiCo_2O_4$ microsphere modified electrodes was higher than that of solid $NiCo_2O_4$ microspheres, Co_3O_4, and NiO microsphere modified electrodes. A similar trend can be found in the SWASV responses of these modified electrodes toward Cu^{II}. Moreover, the stripping peak shifted toward more positive potential in both Pb^{II} and Cu^{II} determination, suggesting that HMIs can be more easily swept from the hollow $NiCo_2O_4$ microsphere modified electrodes compared with other electrodes.[26] Figure 6b shows the SWASV responses of hollow $NiCo_2O_4$ microsphere modified electrode toward Pb^{II} at various concentrations, and the corresponding calibration curve was derived accordingly (inset in Figure 6b). The stripping peak currents are proportional to the concentration of Pb^{II} from 0.2 to 1.2 μM. The linearization equation was $i/\mu A = -2.66 + 26.97c/\mu M$, with a correlation coefficient of 0.994. The limit of detection (LOD) was calculated as 0.089 μM (3σ method), and the sensitivity reached 26.97 $\mu A\ \mu M^{-1}$. The SWASV responses of the hollow $NiCo_2O_4$ microsphere modified electrode toward Cu^{II} over a concentration range of 0.1−1.1 μM are shown in Figure 6c. The linearization equation was $i/\mu A = -1.20 + 12.35c/\mu M$ with a correlation coefficient of 0.992. A sensitivity of 12.35 $\mu A\ \mu M^{-1}$ and a LOD of 0.099 μM (3σ method) were obtained for Cu^{II}. The $NiCo_2O_4$ hollow microsphere modified electrode showed much higher sensitivity than nanoscale carbon, other metal oxides, and nanoscale carbon−metal oxide nanocomposites. For example, it exhibited much higher sensitivity for Pb^{II} detection than O_2-plasma-functionalized multiwalled carbon nanotubes (3.55 $\mu A\ \mu M^{-1}$)[27] and AlOOH-reduced graphene oxide nanocomposites (2.97 $\mu A\ \mu M^{-1}$).[28] Also, it showed higher sensitivity for Cu^{II} detection than SnO_2 tube-in-tube nanostructures (1.54 $\mu A\ \mu M^{-1}$)[7] and SnO_2/reduced graphene oxide nanocomposites (5.17 $\mu A\ \mu M^{-1}$).[29] The selectivity of the hollow $NiCo_2O_4$ microsphere modified electrode was better investigated by observing the stripping currents of six HMIs (Cr^{III}, Zn^{II}, Cd^{II}, Pb^{II}, Cu^{II}, and Hg^{II}; Figure S11 in the SI). It was obvious that the stripping current of 1 μM Pb^{II} or 1.1 μM Cu^{II} was much higher than that of 30-fold other HMIs, indicating the excellent selectivity of this

dx.doi.org/10.1021/am4060707 | ACS Appl. Mater. Interfaces 2014, 6, 3689−3695

electrode toward Pb^{II} and Cu^{II}. To evaluate the stability of the hollow $NiCo_2O_4$ microsphere modified electrode for HMI detection, a series of 20 times repetitive measurements of the SWASV response toward 1.0 μM Cu^{II} were carried out. As shown in Figure 6d, the stripping current of the electrode was highly reproducible with a relative standard deviation of 0.53%. For evaluation of the potential practical application of the modified electrode, a test on the real water samples has been carried out. The real sample was taken from Dongpu Reservoir in Hefei City, Anhui Province, China. The sample water was diluted with a 0.1 M NaAc-HAc solution (pH 5.0) in a ratio of 1:9, and no further treatment was done. Standard additions of Pb^{II} and Cu^{II} were performed in the diluted sample to determine the concentrations of Pb^{II} and Cu^{II} in real water. On the basis of the standard-additions method, the concentrations of Pb^{II} and Cu^{II} in the real sample were calculated to be 3.7 and 2.6 nM. The recovery obtained further demonstrated that the proposed modified electrodes have good practical application potential (Table S1 in the SI). Therefore, the hollow $NiCo_2O_4$ microsphere modified electrode had excellent sensitivity, selectivity, stability, and real application potentials for repetitive stripping measurements of HMIs.

Such remarkable electrochemical performances in methanol electrooxidation and HMIs detection might be attributed to the unique urchin-like $NiCo_2O_4$ hollow structures providing several major advantages, as shown in Figure 7: (1) The high specific surface area and hollow interior increased the contact area of the electrode/electrolyte interface and provided more active sites for electrochemical reactions. (2) The nanorod building blocks can provide an efficient transport path for ions or electrons because of the short diffusion length and high porosity. (3) The higher electronic conductivity of the mixed spinel oxides accelerated the ion or electron transfer at the electrode/electrolyte interface. (4) The synergistic effect of cobalt and nickel species contributed to the higher electrochemical reactivity. The detailed and insightful study into the synergistic effect is ongoing.

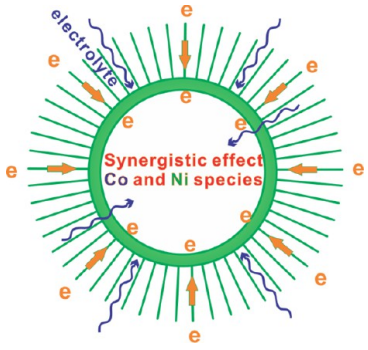

Figure 7. Scheme for the advantages of this novel urchin-like $NiCo_2O_4$ hollow nanostructure.

4. CONCLUSIONS

In summary, we have developed a simple template-free solvothermal method for the synthesis of hierarchical urchin-like $NiCo_2O_4$ hollow microsphere precursors in an IPA–water system. The initially formed microsphere precursors were observed to undergo an interesting hollowing process. These hollow microspheres can be easily converted to $NiCo_2O_4$ hollow microspheres by thermal decomposition with a well-maintained structure. In view of their unique structural advantages, the electrochemical performances of these as-synthesized $NiCo_2O_4$ hollow microspheres were evaluated for methanol oxidation and HMIs detection. The novel urchin-like hollow structures enabled full exposure of the active sites to the electrolyte and provided a short diffusion path for both electrons and ions, thus leading to faster kinetics, lower overpotential and higher electrocatalytic reactivity for methanol oxidation, and higher sensitivity and lower LOD for HMIs detection.

■ ASSOCIATED CONTENT

Supporting Information

SEM image of an individual broken $NiCo_2O_4$ hollow microsphere, XRD patterns and SEM images of hollow $NiCo_2O_4$, solid $NiCo_2O_4$, Co_3O_4, and NiO microspheres precursors and their corresponding oxides, SEM images of $NiCo_2O_4$ precursors prepared under different solvothermal conditions, N_2 adsorption–desorption isotherm of the solid $NiCo_2O_4$ microspheres, EIS plots of $NiCo_2O_4$, Co_3O_4, and NiO modified electrodes, CV curves of modified electrodes (hollow $NiCo_2O_4$, solid $NiCo_2O_4$, Co_3O_4, and NiO) in 1 M KOH with and without 0.5 M methanol, voltammetric peak current of HMIs at the hollow $NiCo_2O_4$ microspheres modified electrode in the presence of Pb^{II}, Cu^{II}, Cr^{III}, Zn^{II}, Cd^{II}, and Hg^{II}, and a table for the determination of Cu^{II} and Pb^{II} in a real sample. This material is available free of charge via the Internet at http://pubs.acs.org.

■ AUTHOR INFORMATION

Corresponding Author

*E-mail: xingjiuhuang@iim.ac.cn. Tel.: +86-551-5591142. Fax: +86-551-5592420.

Author Contributions

‡These two authors contributed equally to this work.

Notes

The authors declare no competing financial interest.

■ ACKNOWLEDGMENTS

The authors acknowledge financial support from the National Key Scientific Program-Nanoscience and Nanotechnology (Grant 2011CB933700) and the National Natural Science Foundation of China (Grants 21103198 and 21073197). X.-J.H. acknowledges the CAS Institute of Physical Science, University of Science and Technology of China (Grant 2012FXCX008), for financial support.

■ REFERENCES

(1) Lou, X. W.; Archer, L. A.; Yang, Z. C. Hollow Micro-/Nanostructures: Synthesis and Applications. *Adv. Mater.* **2008**, *20*, 3987–4019.

(2) Lai, X. Y.; Halpert, J. E.; Wang, D. Recent Advances in Micro-/Nano-Structured Hollow Spheres for Energy Applications: From Simple to Complex Systems. *Energy Environ. Sci.* **2012**, *5*, 9944–9944.

(3) Wang, B.; Wu, H. B.; Yu, L.; Xu, R.; Lim, T. T.; Lou, X. W. Template-free Formation of Uniform Urchin-like α-FeOOH Hollow Spheres with Superior Capability for Water Treatment. *Adv. Mater.* **2012**, *24*, 1111–1116.

(4) Wang, Z. Y.; Wang, Z. C.; Liu, W. T.; Xiao, W.; Lou, X. W. Amorphous $CoSnO_3$@C Nanoboxes with Superior Lithium Storage Capability. *Energy Environ. Sci.* **2013**, *6*, 87–91.

(5) Zhou, L.; Zhao, D. Y.; Lou, X. W. Double-Shelled $CoMn_2O_4$ Hollow Microcubes as High-Capacity Anodes for Lithium-Ion Batteries. *Adv. Mater.* **2012**, *24*, 745−748.
(6) Pan, A. Q.; Wu, H. B.; Zhang, L.; Lou, X. W. Uniform V_2O_5 Nanosheet-Assembled Hollow Microflowers with Excellent Lithium Storage Properties. *Energy Environ. Sci.* **2013**, *6*, 1476−1479.
(7) Chen, X.; Liu, Z. G.; Zhao, Z. Q.; Liu, J. H.; Huang, X. J. SnO_2 Tube-in-Tube Nanostructures: Cu@C Nanocable Templated Synthesis and Their Mutual Interferences between Heavy Metal Ions Revealed by Stripping Voltammetry. *Small* **2013**, *9*, 2233−2239.
(8) Chen, X.; Guo, Z.; Xu, W. H.; Yao, H. B.; Li, M. Q.; Liu, J. H.; Huang, X. J.; Yu, S. H. Templating Synthesis of SnO_2 Nanotubes Loaded with Ag_2O Nanoparticles and Their Enhanced Gas Sensing Properties. *Adv. Funct. Mater.* **2011**, *21*, 2049−2056.
(9) Hu, J.; Chen, M.; Fang, X. S.; Wu, L. W. Fabrication and Application of Inorganic Hollow Spheres. *Chem. Soc. Rev.* **2011**, *40*, 5472−5491.
(10) Lou, X. W.; Wang, Y.; Yuan, C. L.; Lee, J. Y.; Archer, L. A. Template-Free Synthesis of SnO_2 Hollow Nanostructures with High Lithium Storage Capacity. *Adv. Mater.* **2006**, *18*, 2325−2329.
(11) Pan, A. Q.; Wu, H. B.; Yu, L.; Lou, X. W. Template-Free Synthesis of VO_2 Hollow Microspheres with Various Interiors and Their Conversion into V_2O_5 for Lithium-Ion Batteries. *Angew. Chem., Int. Ed.* **2013**, *52*, 2226−2230.
(12) Li, J. F.; Xiong, S. L.; Liu, Y. R.; Ju, Z. C.; Qian, Y. T. High Electrochemical Performance of Monodisperse $NiCo_2O_4$ Mesoporous Microspheres as an Anode Material for Li-Ion Batteries. *ACS Appl. Mater. Interfaces* **2013**, *5*, 981−988.
(13) Qian, L.; Gu, L.; Yang, L.; Yuan, H. Y.; Xiao, D. Direct Growth of $NiCo_2O_4$ Nanostructures on Conductive Substrates with Enhanced Electrocatalytic Activity and Stability for Methanol Oxidation. *Nanoscale* **2013**, *5*, 7388−7396.
(14) Zhang, G. Q.; Lou, X. W. Controlled Growth of $NiCo_2O_4$ Nanorods and Ultrathin Nanosheets on Carbon Nanofibers for High-performance Supercapacitors. *Sci. Rep.* **2013**, *3*, 1470.
(15) Yu, L.; Zhang, G. Q.; Yuan, C. Z.; Lou, X. W. Hierarchical $NiCo_2O_4$@MnO_2 Core-Shell Heterostructured Nanowire Arrays on Ni Foam as High-Performance Supercapacitor Electrodes. *Chem. Commun.* **2013**, *49*, 137−139.
(16) Zhang, G. Q.; Wu, H. B.; Hoster, H. E.; Chan-Park, M. B.; Lou, X. W. Single-Crystalline $NiCo_2O_4$ Nanoneedle Arrays Grown on Conductive Substrates as Binder-free Electrodes for High-Performance Supercapacitors. *Energy Environ. Sci.* **2012**, *5*, 9453−9456.
(17) Zhang, G. Q.; Lou, X. W. General Solution Growth of Mesoporous $NiCo_2O_4$ Nanosheets on Various Conductive Substrates as High-Performance Electrodes for Supercapacitors. *Adv. Mater.* **2013**, *25*, 976−979.
(18) Hu, L. F.; Wu, L. M.; Liao, M. Y.; Hu, X. H.; Fang, X. S. Electrical Transport Properties of Large, Individual $NiCo_2O_4$ Nanoplates. *Adv. Funct. Mater.* **2012**, *22*, 998−1004.
(19) Liu, J.; Liu, C. P.; Wan, Y. L.; Liu, W.; Ma, Z. S.; Ji, S. M.; Wang, J. B.; Zhou, Y. C.; Hodgson, P.; Li, Y. C. Facile Synthesis of $NiCo_2O_4$ Nanorod Arrays on Cu Conductive Substrates as Superior Anode Materials for High-Rate Li-Ion Batteries. *CrystEngComm* **2013**, *15*, 1578−1585.
(20) Liu, Z. Q.; Xu, Q. Z.; Wang, J. Y.; Li, N.; Guo, S. H.; Su, Y. Z.; Wang, H. J.; Zhang, J. H.; Chen, S. Facile Hydrothermal Synthesis of Urchin-like $NiCo_2O_4$ Spheres as Efficient Electrocatalysts for Oxygen Reduction Reaction. *Int. J. Hydrogen Energy* **2013**, *38*, 6657−6662.
(21) Wang, Q. F.; Liu, B.; Wang, X. F.; Ran, S. H.; Wang, L. M.; Chen, D.; Shen, G. Z. Morphology Evolution of Urchin-like $NiCo_2O_4$ Nanostructures and Their Applications as Psuedocapacitors and Photoelectrochemical Cells. *J. Mater. Chem.* **2012**, *22*, 21647−21653.
(22) Anu Prathap, M. U.; Srivastava, R. Synthesis of $NiCo_2O_4$ and Its Application in the Electrocatalytic Oxidation of Methanol. *Nano Energy* **2013**, *2*, 1046−1053.
(23) Wang, L.; Xu, W. H.; Yang, R.; Zhou, T.; Hou, D.; Zheng, X.; Liu, J. H.; Huang, X. J. Electrochemical and Density Functional Theory Investigation on High Selectivity and Sensitivity of Exfoliated Nano-Zirconium Phosphate toward Lead(II). *Anal. Chem.* **2013**, *85*, 3984−3990.
(24) Wei, Y.; Yang, R.; Zhang, Y. X.; Wang, L.; Liu, J. H.; Huang, X. J. High Adsorptive γ-AlOOH(boehmite)@SiO_2/Fe_3O_4 Porous Magnetic Microspheres for Detection of Toxic Metal Ions in Drinking Water. *Chem. Commun.* **2011**, *47*, 11062−11064.
(25) Zhao, Z. Q.; Chen, X.; Yang, Q.; Liu, J. H.; Huang, X. J. Selective Adsorption toward Toxic Metal Ions Results in Selective Response: Electrochemical Studies on a Polypyrrole/Reduced Graphene Oxide Nanocomposite. *Chem. Commun.* **2012**, *48*, 2180−2182.
(26) Yu, X. Y.; Meng, Q. Q.; Luo, T.; Jia, Y.; Sun, B.; Li, Q. X.; Liu, J. H.; Huang, X. J. Facet-Dependent Electrochemical Properties of Co_3O_4 Nanocrystals toward Heavy Metal Ions. *Sci. Rep.* **2013**, *3*, 2886.
(27) Wei, Y.; Liu, Z.-G.; Yu, X.-Y.; Wang, L.; Liu, J.-H.; Huang, X.-J. O_2-Plasma Oxidized Multi-Walled Carbon Nanotubes for Cd(II) and Pb(II) Detection: Evidence of Adsorption Capacity for Electrochemical Sensing. *Electrochem. Commun.* **2011**, *13*, 1506−1509.
(28) Gao, C.; Yu, X. Y.; Xu, R. X.; Liu, J. H.; Huang, X. J. AlOOH-Reduced Graphene Oxide Nanocomposites: One-Pot Hydrothermal Synthesis and Their Enhanced Electrochemical Activity for Heavy Metal Ions. *ACS Appl. Mater. Interfaces* **2012**, *4*, 4672−82.
(29) Wei, Y.; Gao, C.; Meng, F.-L.; Li, H.-H.; Wang, L.; Liu, J.-H.; Huang, X.-J. SnO_2/Reduced Graphene Oxide Nanocomposite for the Simultaneous Electrochemical Detection of Cadmium(II), Lead(II), Copper(II), and Mercury(II): An Interesting Favorable Mutual Interference. *J. Phys. Chem. C* **2012**, *116*, 1034−1041.